Journal of Solid State Chemistry 183 (2010) 909–914

Contents lists available at ScienceDirect

Journal of Solid State Chemistry

journal homepage: www.elsevier.com/locate/jssc

Origin of periodic domain structure in Er^{3+}-doped β′-$(Sm,Gd)_2(MoO_4)_3$ crystal lines patterned by laser irradiations in glasses

Futoshi Suzuki, Tsuyoshi Honma, Takayuki Komatsu *

Department of Materials Science and Technology, Nagaoka University of Technology, 1603-1 Kamitomioka-cho, Nagaoka 940-2188, Japan

ARTICLE INFO

Article history:
Received 30 November 2009
Received in revised form
4 February 2010
Accepted 9 February 2010
Available online 17 February 2010

Keywords:
β′-$Gd_2(MoO_4)_3$
Ferroelasticity
Domain structure
Er^{3+}-doping
Crystallization
Laser patterning

ABSTRACT

Er^{3+}-doped β′-$(Sm,Gd)_2(MoO_4)_3$ crystal lines are patterned on the surface of Er_2O_3–Gd_2O_3–Sm_2O_3–MoO_3–B_2O_3 glasses by continuous-wave Yb:YVO_4 laser irradiations (wavelength: 1080 nm, power: 1.3 W, scanning speeds: 5 μm/s), and the origin of the periodicity of self-organized domain structures with high and low refractive index regions in crystal lines is examined from polarized optical microscope (POM) observations, micro-Raman scattering spectrum, and photoluminescence spectrum measurements. It is found that the periodicity of domain structures changes largely depending on Er_2O_3 content, i.e., the length of high (bright color in POM observations) and low (dark color) refractive index regions increases with increasing Er_2O_3 content and homogeneous crystal lines with no periodic domain structures are patterned in Er_2O_3–Sm_2O_3–MoO_3–B_2O_3 glass with no Gd_2O_3. Considering that the degree of ferroelasticities in β′-$(Sm,Gd)_2(MoO_4)_3$ crystals decreases due to the incorporation of Er^{3+} ions, it is demonstrated that the origin of periodic domain structures in laser-patterned lines is due to spontaneous strains in ferroelastic β′-$(Sm,Gd)_2(MoO_4)_3$ crystals.

1. Introduction

Acentric rare-earth molybdates, β′-$RE_2(MoO_4)_3$, (RE: Pr, Nd, Sm, Eu, Gd, Tb, Dy), with an orthorhombic structure (*Pba*2) are well-known unique crystals possessing both ferroelectricity and ferroelasticity, giving potentials for optical device applications [1–8]. Very recently, Tsukada et al. [9,10] found the formation of periodic domain structures with high (bright color in polarized optical microscope (POM) observations) and low (dark color) refractive index regions in ferroelastic β′-$(Sm,Gd)_2(MoO_4)_3$, designated here as SGMO, crystal lines patterned on the surface of Sm_2O_3–Gd_2O_3–MoO_3–B_2O_3 glasses by continuous-wave (cw) Yb:YVO_4 laser irradiations (wavelength: λ=1080 nm). The intensity of second harmonic (SH) waves generating from SGMO crystal lines changes periodically depending on unique periodic domain structures. A similar unique domain structure has been found in β′-$Gd_2(MoO_4)_3$, designated here as GMO, crystal grains which are obtained in usual crystallizations in an electric furnace [11]. It is of interest and important to characterize morphologies and optical properties of β′-$RE_2(MoO_4)_3$ crystal lines from scientific and device application points of view and to clarify the origin of periodic domain structures in laser-patterned β′-$RE_2(MoO_4)_3$ crystal lines. Tsukada et al. [9,10] proposed that the origin of periodic domain structures in laser-patterned β′-$(Sm,Gd)_2(MoO_4)_3$ crystal lines might be due to spontaneous strains in ferroelastic β′-$(Sm,Gd)_2(MoO_4)_3$ crystals. At this moment, however, the presence of spontaneous strains in laser-patterned lines has not been demonstrated experimentally due to the lack of proper experimental techniques.

The crystal structure and properties of $RE_2(MoO_4)_3$ crystals depend on the kind of RE elements. For instance, for Gd^{3+} ions, the crystalline phase of β′-$Gd_2(MoO_4)_3$ showing a strong ferroelasticity is present [1–8], but for Er^{3+} ions the presence of ferroelastic β′-$Er_2(MoO_4)_3$ crystals has not been reported. It is, therefore, expected that the doping of other RE^{3+} ions such as Er^{3+} into GMO crystals induces large changes in their ferroelasticities and optical properties. In other words, the periodic domain structure in laser patterned GMO crystal lines would be largely affected due to the incorporation of Er^{3+} ions, if certainly the origin of periodic domain structures is due to spontaneous strains in GMO crystals. Therefore, the study on the laser patterning of Er^{3+}-doped GMO crystal lines and their morphologies would be a good approach for understanding and demonstrating the origin of periodic domain structures more clearly. Furthermore, it is of interest to confirm the incorporation of Er^{3+} ions into GMO crystal lines, because Er^{3+} is one of the important rare-earth ions giving excellent photoluminescence (PL) properties in optical materials and devices.

In this study, Er^{3+}-doped β′-$(Sm,Gd)_2(MoO_4)_3$ crystal lines are patterned on the surface of Er_2O_3–Gd_2O_3–Sm_2O_3–MoO_3–B_2O_3 glasses by cw Yb:YVO_4 laser irradiations, and the effect of Er^{3+} doping on the morphology and optical properties of crystal lines is examined to demonstrate the origin of self-organized periodic

* Corresponding author. Fax: +81 258 47 9300.
E-mail address: komatsu@mst.nagaokaut.ac.jp (T. Komatsu).

0022-4596/$ - see front matter © 2010 Elsevier Inc. All rights reserved.
doi:10.1016/j.jssc.2010.02.007

domain structures in laser-patterned β′-$(Sm,Gd)_2(MoO_4)_3$ lines. The present study indicates that the periodicity of domain structures changes depending on the amount of Er^{3+} addition, i.e., the length of high (bright color) and low (dark color) refractive index regions increases with increasing Er_2O_3 content and homogeneous crystal lines with no periodic domain structures are patterned in Er_2O_3–Sm_2O_3–MoO_3–B_2O_3 glass with no Gd_2O_3. Laser irradiation to glass has been regarded as a process for spatially selected structural modification and/or crystallization in glass, and laser-induced crystallization techniques have been applied to various glasses in order to pattern functional crystals in glasses [12–15]. The control of the morphology of laser-patterned crystal lines would give a great contribution on material science and technology.

2. Experimental

Glasses with the compositions of xEr_2O_3–$(18.25-x)Gd_2O_3$–$3Sm_2O_3$–$63.75MoO_3$–$15B_2O_3$ (mol%), x=0, 3, 7.625, and 18.25, were prepared using a conventional melt quenching technique. It has been reported that β′-$RE_2(MoO_4)_3$ crystals are synthesized through the crystallization of $21.25RE_2O_3$–$63.75MoO_3$–$15B_2O_3$ glasses in an electric furnace [16–18]. A small amount (3 mol%) of Sm_2O_3 was added to absorb Yb:YVO_4 laser light and to transfer laser energies to thermal energies, i.e., to the laser patterning of β′-$(Sm,Gd)_2(MoO_4)_3$ crystal lines [9,10,12]. Commercial powders of reagent grade Er_2O_3, Gd_2O_3, Sm_2O_3, MoO_3, and H_3BO_3 were used as starting materials. A mixed batch of 15 g in weight was melted in a platinum crucible at 1100 °C for 30 min in an electric furnace. The melts were poured onto an iron plate and pressed to a thickness of ~1.5 mm by another iron plate. The glass transition, T_g, and crystallization peak, T_p, temperatures were determined using a differential thermal analysis (DTA) at heating rate of 10 K/min. Glasses were mechanically polished to a mirror finish with CeO_2 powders. The quenched glasses were annealed at T_g for 30 min to release internal stresses. The glasses were heat-treated at around T_p, and the crystalline phases present in the crystallized samples were identified by X-ray diffraction (XRD) analysis (Cu$K\alpha$ radiation) at room temperature. Second harmonic generations (SHGs) for crystallized samples were examined using a SHG microscope [19].

A cw Yb:YVO_4 fiber laser with λ=1080 nm was irradiated onto the glass surface. The laser beam was focused on the surface of glasses using an objective lens (magnification: 50 times, numerical aperture: NA=0.8). The plate shape glasses were put on the stage and mechanically moved during laser irradiations to construct crystal lines. The laser power was 1.3 W, and a translation speed of the sample stage, i.e., scanning speed of laser, was 5 μm/s. The surface morphology of lines patterned by Yb:YVO_4 fiber laser irradiations was examined from POM observations. Micro-Raman scattering spectra and PL spectra at room temperature for laser-patterned crystal lines were taken with a laser microscope (Tokyo Instruments Co., Nanofinder) operated at Ar^+ (488 nm, 10 mW) laser.

3. Results and discussion

3.1. Thermal properties and crystallization of Er^{3+}-doped bulk glasses

Prior to the laser patterning of Er^{3+}-doped β′-$(Sm,Gd)_2(MoO_4)_3$ crystal lines, the effect of Er^{3+} doping on the thermal stability and crystallization behavior of xEr_2O_3–$(18.25-x)Gd_2O_3$–$3Sm_2O_3$–$63.75MoO_3$–$15B_2O_3$ (mol%) glasses was examined. All melt-quenched samples show good optical transparency and show only broad halo patterns in XRD patterns. The DTA patterns in air for the glasses with x=0, 3, 7.625, and 18.25 are shown in Figs. 1 and 2, where endothermic peaks corresponding to the glass transition and exothermic peaks due to the crystallization are clearly observed. It is, therefore, concluded that clear glasses were obtained for all samples with x=0–18.25. As can be seen in Fig. 2, the bulk sample with x=18.25 with no Gd_2O_3 shows an unusual DTA pattern. As will be described later, the bulk glasses with x=0, 3, and 7.625 show the crystallization of ferroelastic β′-$RE_2(MoO_4)_3$, but the glass with x=18.25 gives the formation of $Er_2(MoO_4)_3 \cdot 3H_2O$ crystals containing H_2O molecules. It is considered that the unusual DTA pattern in Fig. 2 might be related to a unique crystallization behavior of the glass with a large amount of Er_2O_3. The values of T_g~528 °C and T_p~580 °C are obtained for the glasses with x=0, 3, and 7.625.

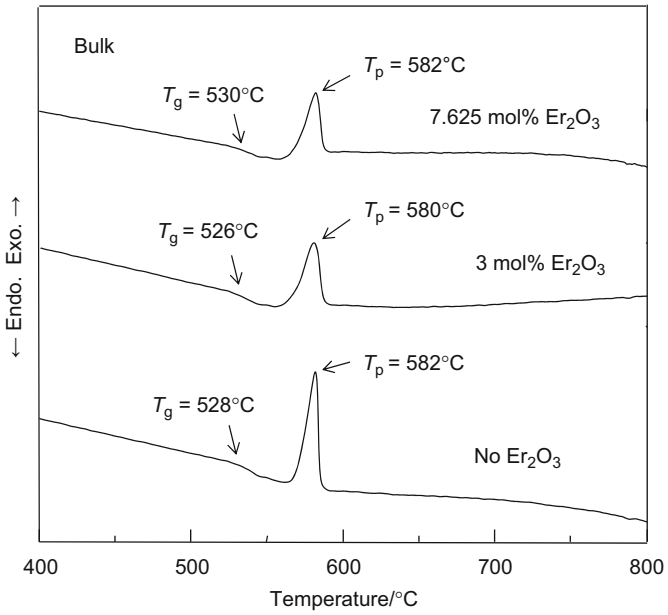

Fig. 1. DTA patterns in air for xEr_2O_3–$(18.25-x)Gd_2O_3$–$3Sm_2O_3$–$63.75MoO_3$–$15B_2O_3$ (mol%) glasses (bulk samples) with x=0, 3 and 7.625. T_g and T_p are the glass transition and crystallization peak temperatures respectively. Heating rate was 10 K/min.

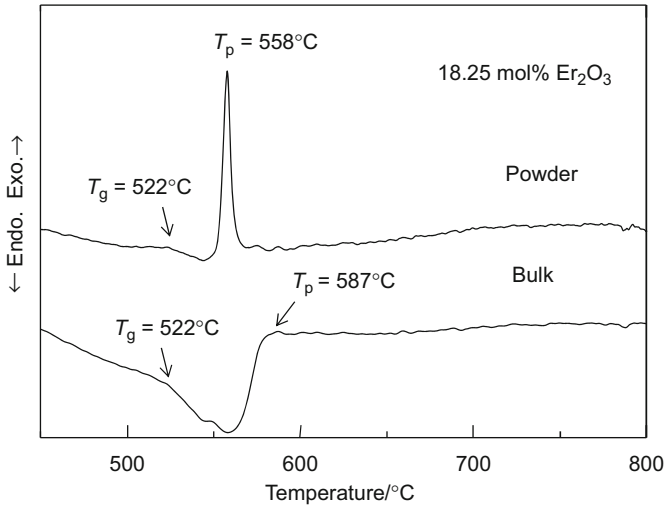

Fig. 2. DTA patterns in air for $18.25Er_2O_3$–$3Sm_2O_3$–$63.75MoO_3$–$15B_2O_3$ (mol%) glass (powder and bulk samples). T_g and T_p are the glass transition and crystallization peak temperatures, respectively. Heating rate was 10 K/min.

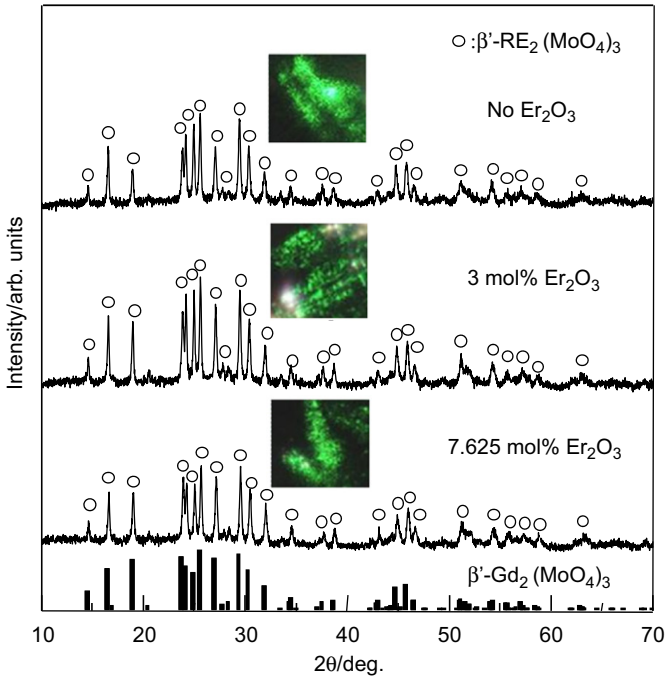

Fig. 3. XRD patterns at room temperature for the crystallized (at T_p for 2 h in air) samples of $x\mathrm{Er_2O_3}$–$(18.25-x)\mathrm{Gd_2O_3}$–$3\mathrm{Sm_2O_3}$–$63.75\mathrm{MoO_3}$–$15\mathrm{B_2O_3}$ (mol%) glasses. All peaks are assigned to β′-$\mathrm{RE_2(MoO_4)_3}$ crystals. The XRD pattern for β′-$\mathrm{Gd_2(MoO_4)_3}$ crystals (JCPDS: No. 01-071-0915) is also included.

The XRD patterns for the crystallized (at T_p for 2 h in air) samples with x=0, 3, and 7.625 are shown in Fig. 3, in which the XRD pattern for β′-$\mathrm{Gd_2(MoO_4)_3}$ crystals (JCPDS: No. 01-071-0915 and Ref. [18]) is included. The data on the sample with x=18.25 will be described later. All peaks in Fig. 3 are assigned to β′-$\mathrm{RE_2(MoO_4)_3}$ crystals. In previous studies [9,10,16,17], it has been reported that β′-$\mathrm{(Sm,Gd)_2(MoO_4)_3}$ crystals are formed in the crystallization of $18.25\mathrm{Gd_2O_3}$–$3\mathrm{Sm_2O_3}$–$63.75\mathrm{MoO_3}$–$15\mathrm{B_2O_3}$ (mol%) glass. In $\mathrm{Er_2O_3}$-doped samples, the position of diffraction peaks was found to shift toward higher angles with increasing $\mathrm{Er_2O_3}$ content. The XRD patterns in the angle of 2θ=24.5–26° are shown in Fig. 4 in order to find the shifts more clearly.

The ionic radii of Gd^{3+} and Er^{3+} with seven oxygen coordinations are 0.100 and 0.0945 nm, respectively [20], and it is, therefore, considered that Er^{3+} ions are incorporated into β′-$\mathrm{(Sm,Gd)_2(MoO_4)_3}$ crystals, i.e., the formation of Er^{3+}-doped β′-$\mathrm{(Sm,Gd)_2(MoO_4)_3}$ crystals. The lattice constants of a, b and c in Er^{3+}-doped β′-$\mathrm{(Sm,Gd)_2(MoO_4)_3}$ crystals with an orthorhombic structure formed in the crystallized samples are evaluated from the least square method, in which ten peaks with strong intensities such as (111), (002), (220), and (203) were used. The values evaluated are given in Fig. 5 as a function of $\mathrm{Er_2O_3}$ content. It is seen that all parameters of a, b and c decrease and in particular the difference between a and b decreases with increasing $\mathrm{Er_2O_3}$ content. It has been suggested that the degree of spontaneous strain χ_s in ferroelastic β′-$\mathrm{RE_2(MoO_4)_3}$ crystals is related to lattice parameters through the relation $\chi_s=(b-a)/(a+b)$, indicating that the large difference between a and b induces large spontaneous strains [2]. The data shown in Figs. 3–5, therefore, suggest that the incorporation of Er^{3+} into β′-$\mathrm{(Sm,Gd)_2(MoO_4)_3}$ crystals leads to the decrease in their ferroelasticities. The microscope observations of SHGs for the Er^{3+}-doped crystallized samples are shown in Fig. 3. Clear green light is observed even in the samples with $\mathrm{Er_2O_3}$ contents of 3 and 7.625 mol%, demonstrating that the Er^{3+}-doped β′-$\mathrm{(Sm,Gd)_2(MoO_4)_3}$ crystals formed in the present study are still nonlinear optical crystals.

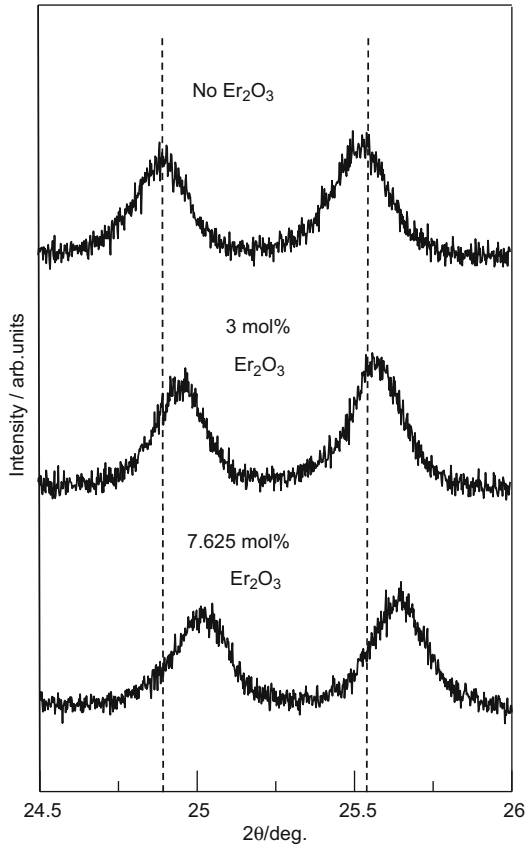

Fig. 4. XRD patterns in the angle of 2θ=24.5–26° at room temperature for the crystallized (at T_p for 2 h in air) samples of $x\mathrm{Er_2O_3}$–$(18.25-x)\mathrm{Gd_2O_3}$–$3\mathrm{Sm_2O_3}$–$63.75\mathrm{MoO_3}$–$15\mathrm{B_2O_3}$ (mol%) glasses.

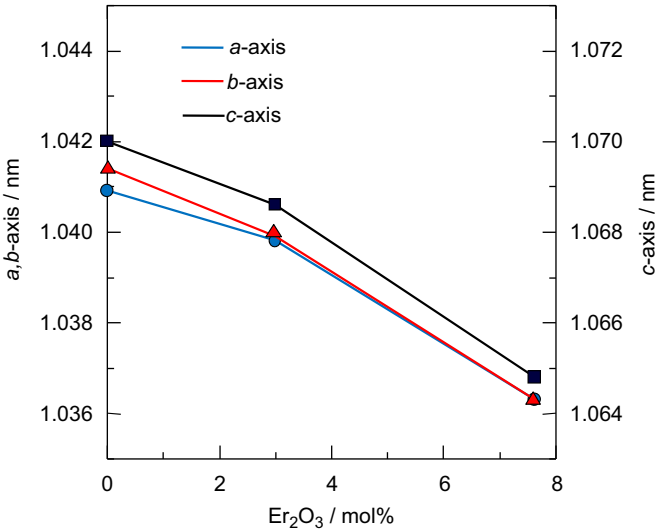

Fig. 5. Lattice constants of a, b and c of Er^{3+}-doped β′-$\mathrm{(Sm,Gd)_2(MoO_4)_3}$ crystals with an orthorhombic structure in the crystallized samples as a function of $\mathrm{Er_2O_3}$ content. The error in a, b and c was within 0.3%.

3.2. *Laser patterning of Er^{3+}-doped β′-$Gd_2(MoO_4)_3$ crystal lines*

In previous studies [9,10], it has been reported that β′-$\mathrm{(Sm,Gd)_2(MoO_4)_3}$ crystal lines with periodic domain structures with high (bright color in POM observations) and low (dark color) refractive index regions are patterned constantly on the glass surface by Yb:$\mathrm{YVO_4}$ laser irradiations with the condition of the

laser power of P=1.3 W and scanning speed of S=5 μm/s. In the present study, we used this laser irradiation condition for the patterning of Er^{3+}-doped β′-$(Sm,Gd)_2(MoO_4)_3$ crystal lines. It should be pointed out that Er^{3+} ions have no absorption due to the f–f transition for the wavelength of 1080 nm, which corresponds to the wavelength of Yb:YVO_4 laser, and that the amount of Sm_2O_3 content in xEr_2O_3–$(18.25-x)Gd_2O_3$–$3Sm_2O_3$–$63.75MoO_3$–$15B_2O_3$ (mol%) glasses is constant. In other words, laser irradiation with P=1.3 W and S=5 μm/s is expected to give a similar thermal heating effect in the glasses prepared in this study. It should be also pointed out that the glass transition and crystallization temperatures are almost the same irrespective of Er_2O_3 content. Therefore, it is expected that the laser irradiation condition of P=1.3 W and S=5 μm/s induces almost the same heating and thus crystallization effect for all xEr_2O_3–$(18.25-x)Gd_2O_3$–$3Sm_2O_3$–$63.75MoO_3$–$15B_2O_3$ (mol%) glasses.

The polarized optical photographs (top view) for the lines patterned by laser irradiations with P=1.3 W and S=5 μm/s for the glasses with x=0, 3 and 7.625 are shown in Fig. 6. Structural changes are clearly induced along the laser scanning direction in all samples, and the periodic structural changes with bright (high refractive index) and dark (low refractive index) color regions are observed. In previous papers [9,10], these periodic structural changes were proposed to call "self-organized periodic domains". The width of lines is about 4 μm, almost irrespective of Er^{3+} content. On the other hand, the length of bright and dark color regions changes depending on Er^{3+} content. In particular, it is noted that those lengths increase with increasing Er^{3+} content. For instance, in 3 mol% Er_2O_3 content, the lengths of bright and dark color regions are 25–36 and 14–25 μm, respectively, and in 7.625 mol% Er_2O_3 content, they are 65–117 and 20–38 μm, respectively.

The micro-Raman scattering spectra at room temperature for bright and dark color regions of the laser-patterned (P=1.3 W, S=5 μm/s) lines in the glasses with no Er_2O_3 and 7.625 mol% Er_2O_3 are shown in Figs. 7 and 8. As a reference, the Raman scattering spectrum at room temperature for β′-$Gd_2(MoO_4)_3$ crystals obtained by the crystallization (590 °C, 2 h) of $21.25Gd_2O_3$–$63.75MoO_3$–$15B_2O_3$ (mol%) glass is shown in Fig. 9. All Raman peaks observed for the lines in Figs. 7 and 8 are assigned to bending or stretching vibrations of Mo–O bonds in $(MoO_4)^{2-}$ tetrahedra of β′-$RE_2(MoO_4)_3$ crystals [21–23]. It is, therefore, concluded that bright and dark color regions in the laser-patterned lines consist of β′-$(Sm,Gd)_2(MoO_4)_3$ crystals

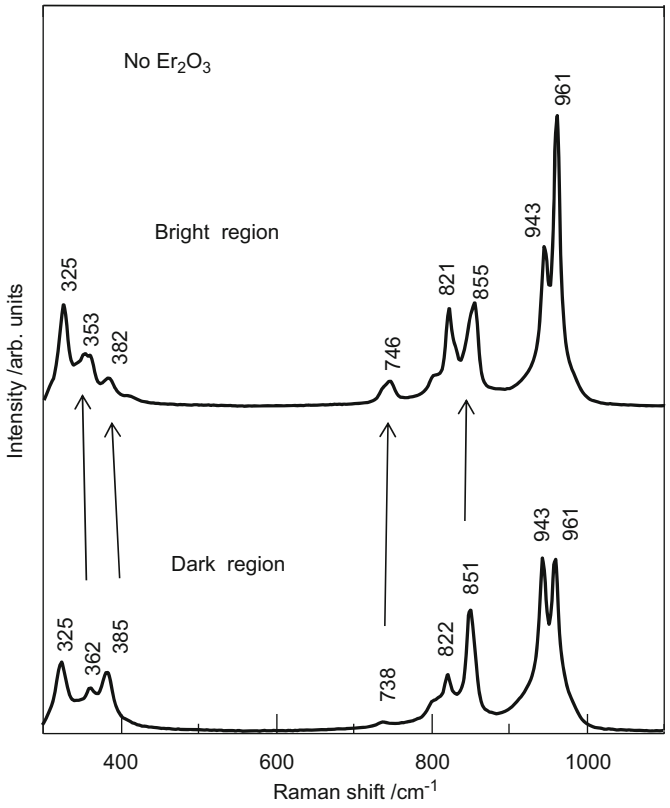

Fig. 7. Micro-Raman scattering spectra at room temperature for bright and dark color regions of the laser-patterned (P=1.3 W, S=5 μm/s) line in $18.25Gd_2O_3$–$3Sm_2O_3$–$63.75MoO_3$–$15B_2O_3$ (mol%) glass.

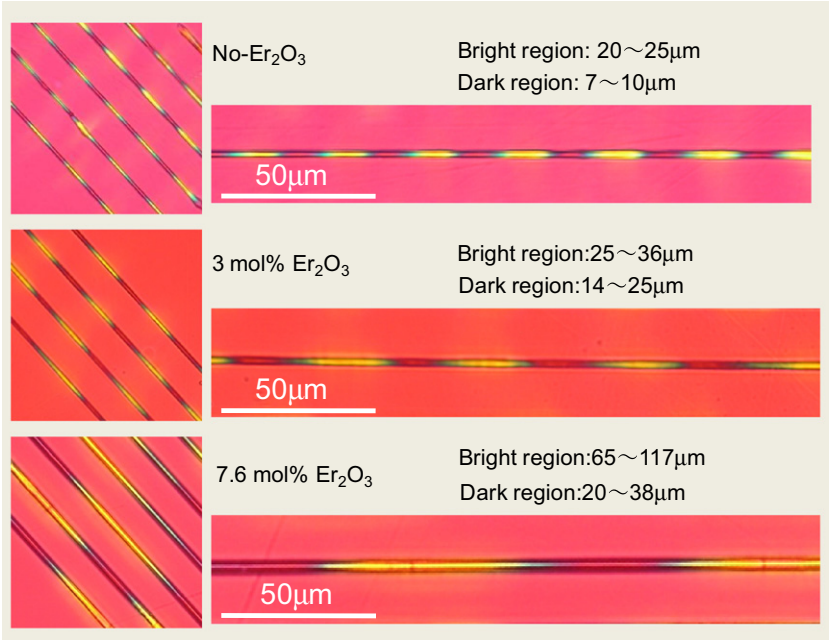

Fig. 6. Polarized optical photographs (top view) for the lines patterned by laser irradiations with the power of P=1.3 W and the scanning speed of S=5 μm/s in xEr_2O_3–$(18.25-x)Gd_2O_3$–$3Sm_2O_3$–$63.75MoO_3$–$15B_2O_3$ (mol%) glasses.

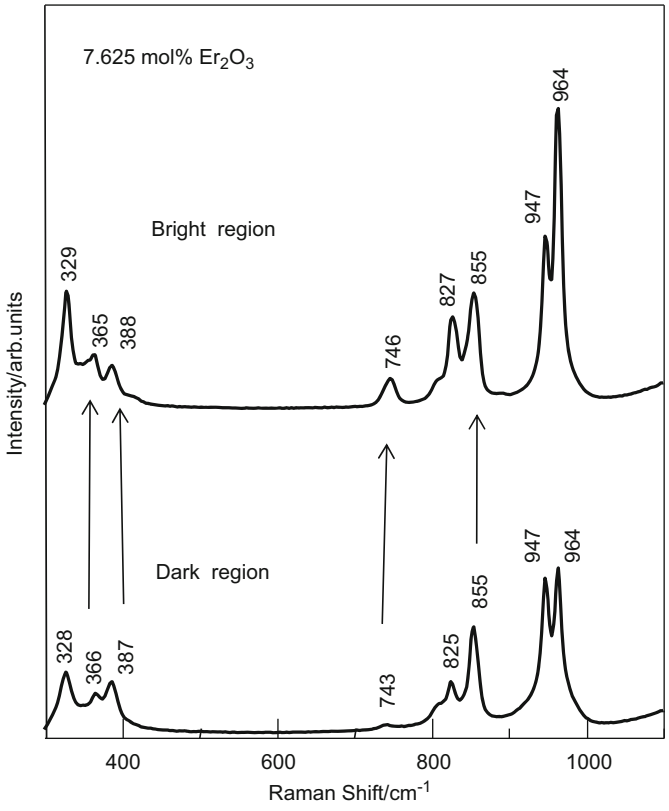

Fig. 8. Micro-Raman scattering spectra at room temperature for bright and dark color regions of the laser-patterned (P=1.3 W, S=5 μm/s) line in 7.625Er_2O_3–10.65Gd_2O_3–3Sm_2O_3–63.75MoO_3–15B_2O_3 (mol%) glass.

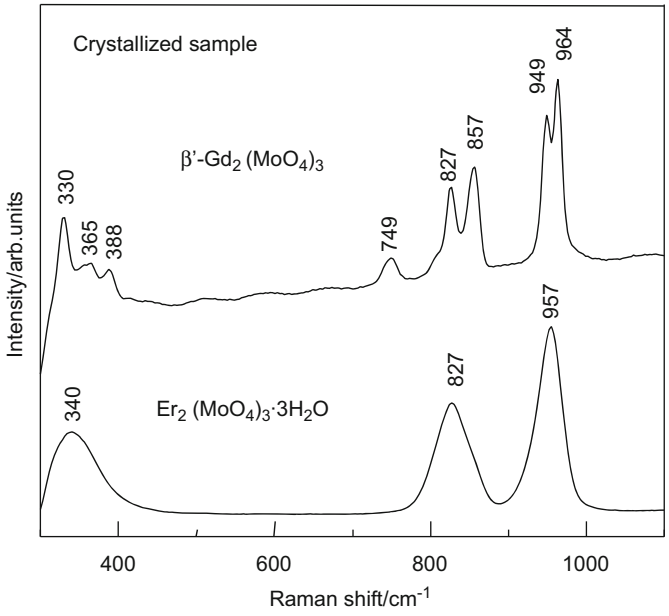

Fig. 9. Raman scattering spectra at room temperature for β′-$Gd_2(MoO_4)_3$ and $Er_2(MoO_4)_3 \cdot 3H_2O$ crystals obtained by the crystallization (590 °C, 2 h) of $x$$Er_2O_3$–(21.25 − x)Gd_2O_3–63.75MoO_3–15B_2O_3 (mol%) glasses with x=0 and 21.25.

irrespective of Er_2O_3 content (0–7.625 mol%). As can be seen in Figs. 7 and 8, the peak positions in the bright color region are different from those in the dark color region. For instance, for the line of the glass with no Er_2O_3, the bright region gives the peaks at 382, 746, and 855 cm^{-1}, but the dark region shows the peaks at 385, 738 and 851 cm^{-1}. On the other hand, for the line of the glass with 7.625 mol% Er_2O_3, the bright region gives the peaks at 388, 746, and 855 cm^{-1}, but the dark region shows the peaks at 387, 743 and 855 cm^{-1}. That is, the difference in the peak position between the bright and dark color regions for the line of the glass with no Er_2O_3 is large compared with the line of the glass with 7.625 mol% Er_2O_3. It is well known that Raman peak position generally shifts due to the presence of strains loaded to crystal structure. The results shown in Figs. 7 and 8 strongly suggest that the degree of spontaneous strains in ferroelastic β′-$(Sm,Gd)_2(MoO_4)_3$ crystals in laser-patterned lines changes due to the substitution of Er_2O_3 for Gd_2O_3.

The PL spectra at room temperature for bright and dark color regions of the line patterned by laser irradiations (P=1.3 W, S=5 μm/s) for 7.625 mol% Er_2O_3 doped glass are shown in Fig. 10. The PL spectrum for the glass part (non-laser irradiated region) is also included in Fig. 10. It is found that both bright and dark color regions give sharp PL peaks corresponding to the f–f transitions of $^2H_{11/2} \rightarrow {}^4I_{15/2}$ and $^4S_{3/2} \rightarrow {}^4I_{15/2}$ for Er^{3+} ions, i.e., Stark splitting peaks [24–27]. Furthermore, it should be pointed out that the PL spectra in the bright color region are slightly different from those in the dark color region, suggesting the difference in the coordination or bonding state of Er^{3+} ions between bright and dark color regions. Anyway, the PL spectra shown in Fig. 10 suggest that Er^{3+} ions are incorporated into β′-$(Sm,Gd)_2(MoO_4)_3$ crystals. Recently, Pan and Zhang [28] synthesized Er^{3+}-doped $Gd_2(MoO_4)_3$ nanocrystals with an orthorhombic structure and reported intense green emission peaks at 525 and 544 nm attributed to the f–f transitions of $^2H_{11/2} \rightarrow {}^4I_{15/2}$ and $^4S_{3/2} \rightarrow {}^4I_{15/2}$ for Er^{3+} ions.

The XRD pattern at room temperature for the crystallized (590 °C, 2 h) sample in 18.25Er_2O_3–3Sm_2O_3–63.75MoO_3–15B_2O_3 (mol%) glass with no Gd_2O_3 is shown in Fig. 11. The formation of $Er_2(MoO_4)_3 \cdot 3H_2O$ crystals [29,30] is confirmed. The Raman scattering spectrum at room temperature for the crystallized sample is also shown in Fig. 9, indicating that $Er_2(MoO_4)_3 \cdot 3H_2O$ crystals give different Raman peaks compared with ferroelastic β′-$Gd_2(MoO_4)_3$ crystals. Because $Er_2(MoO_4)_3$ crystal is hydroscopic [29,30], $Er_2(MoO_4)_3$ crystals formed in the crystallization might absorb water molecules at room temperature after crystallization, transforming into hydrated $Er_2(MoO_4)_3 \cdot 3H_2O$ crystals. It should be pointed out that the

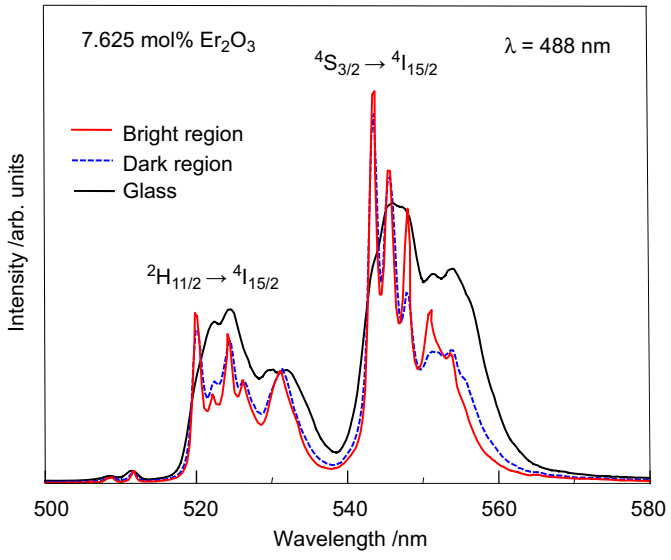

Fig. 10. Photoluminescence spectra at room temperature for bright and dark color regions of the line patterned by laser irradiations (P=1.3 W, S=5 μm/s) for 7.625 mol% Er_2O_3 doped glass.

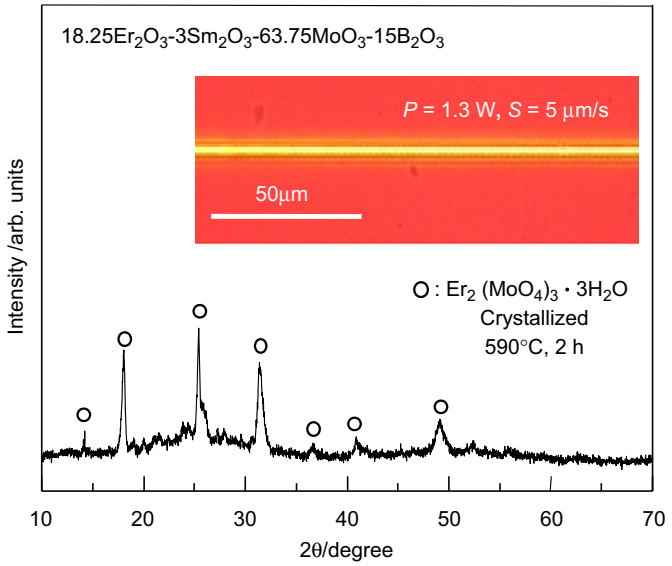

Fig. 11. XRD pattern at room temperature for the crystallized (at 590 °C for 2 h in air) sample of $18.25Er_2O_3$–$3Sm_2O_3$–$63.75MoO_3$–$15B_2O_3$ (mol%) glass. All peaks are assigned to $Er_2(MoO_4)_3 \cdot 3H_2O$ crystals. The polarized optical photograph (top view) for the line patterned by laser irradiations (P=1.3 W, S=5 μm/s) is also included.

presence of the crystalline phase β′-$Er_2(MoO_4)_3$ has not been reported so far. We also carried out laser irradiations (P=1.3 W, S=5 μm/s) to this glass with no Gd_2O_3, and the result is shown in Fig. 11. It is found that a homogeneous crystal line with no periodic domain structures is patterned. Considering that $Er_2(MoO_4)_3$ and $Er_2(MoO_4)_3 \cdot 3H_2O$ crystals are not ferroelastic and thus spontaneous strains are not induced in the inside of crystals, it is expected that periodic domain structures would not generate in laser-patterned lines in $18.25Er_2O_3$–$3Sm_2O_3$–$63.75MoO_3$–$15B_2O_3$ (mol%) glass.

The results obtained in the present study indicate that Er^{3+}-doped β′-$(Sm,Gd)_2(MoO_4)_3$ crystals are patterned by laser irradiations in xEr_2O_3–$(18.25-x)Gd_2O_3$–$3Sm_2O_3$–$63.75MoO_3$–$15B_2O_3$ (mol%) glasses with x=3 and 7.625 and the degree of spontaneous strains in β′-$(Sm,Gd)_2(MoO_4)_3$ crystals decreases with Er^{3+} doping. And consequently, the periodicity of bright and dark color regions in laser-patterned lines changes with the substitution of Er_2O_3 for Gd_2O_3, as shown in Fig. 6. That is, the present study demonstrates more clearly the origin of periodic domain structures in laser-patterned lines consisting of β′-$(Sm,Gd)_2(MoO_4)_3$ crystals, i.e., the periodic domain structure is formed due to spontaneous strains in ferroelastic β′-$(Sm,Gd)_2(MoO_4)_3$ crystals.

4. Conclusions

Ferroelastic β′-$(Sm,Gd)_2(MoO_4)_3$ crystal lines were patterned on the surface of xEr_2O_3–$(18.25-x)Gd_2O_3$–$3Sm_2O_3$–$63.75MoO_3$–$15B_2O_3$ (mol%) glasses with x=0, 3, 7.625, and 18.25 by continuous-wave Yb:YVO_4 laser irradiations (wavelength: 1080 nm, power: 1.3 W, scanning speeds: 5 μm/s) in order to clarify the origin of the periodicity of self-organized domain structures appeared in crystal lines. It was found from polarized optical microscope observations, micro-Raman scattering spectrum, and photoluminescence spectrum measurements that Er^{3+} ions are incorporated into β′-$(Sm,Gd)_2(MoO_4)_3$ crystals and the periodicity of domain structures changes largely depending on Er_2O_3 content. It was demonstrated that the origin of periodic domain structures in laser-patterned lines is due to spontaneous strains in ferroelastic β′-$RE_2(MoO_4)_3$ crystals.

Acknowledgments

This work was supported from the Grant-in-Aid for Scientific Research from the Ministry of Education, Science, Sports, Culture and Technology, Japan.

References

[1] H.J. Borchardt, P.E. Bierstedt, Appl. Phys. Lett. 8 (1966) 50.
[2] K. Aizu, A. Kumada, H. Yumoto, S. Ashida, J. Phys. Soc. Jpn. 27 (1969) 511.
[3] E.T. Keve, S.C. Abrahams, J.L. Bernstein, J. Chem. Phys. 54 (1971) 3185.
[4] K. Nassau, J.W. Shiever, E.T. Keve, J. Solid State Chem. 3 (1971) 411.
[5] W. Jeitschko, Acta Cryst. B 28 (1972) 60.
[6] A. Kumada, Ferroelectrics 3 (1972) 115.
[7] A.N. Alexeyev, D.V. Roshchupkin, Appl. Phys. Lett. 68 (1996) 159.
[8] H. Nishioka, W. Odajima, M. Tateno, K. Ueda, A.A. Kaminskii, A.V. Butashin, S.N. Bagayev, A.A. Pavlyuk, Appl. Phys. Lett. 70 (1997) 1366.
[9] Y. Tsukada, T. Honma, T. Komatsu, Appl. Phys. Lett. 94 (2009) 059901.
[10] T. Honma, Y. Tsukada, T. Komatsu, Opt. Mater. 32 (2010) 443.
[11] Y. Tsukada, T. Honma, T. Komatsu, J. Solid State Chem. 182 (2009) 2269.
[12] T. Komatsu, R. Ihara, T. Honma, Y. Benino, R. Sato, H.G. Kim, T. Fujiwara, J. Am. Ceram. Soc. 90 (2007) 699.
[13] B. Franta, T. Williams, C. Faris, S. Feller, M. Affatigao, Phys. Chem. Glasses: Eur. J. Glass Sci. Technol. B 48 (2007) 357.
[14] Y. Dai, B. Zhu, J. Qiu, H. Ma, B. Lu, B. Yu, Chem. Phys. Lett. 443 (2007) 253.
[15] P. Gupta, H. Jain, D.B. Williams, T. Honma, Y. Benino, T. Komatsu, J. Am. Ceram. Soc. 91 (2008) 110.
[16] M. Abe, Y. Benino, T. Fujiwara, T. Komatsu, R. Sato, J. Appl. Phys. 97 (2005) 123516.
[17] R. Nakajima, M. Abe, Y. Benino, T. Fujiwara, H.G. Kim, T. Komatsu, J. Non-Cryst. Solids 353 (2007) 85.
[18] R. Nakajima, T. Honma, Y. Benino, T. Komatsu, J. Ceram. Soc. Jpn. 115 (2007) 582.
[19] T. Fujiwara, T. Sawada, T. Honma, Y. Benino, T. Komatsu, M. Takahashi T. Yoko, J. Nishii, Jpn. J. Appl. Phys. 42 (2003) 7326.
[20] R.D. Shannon, Acta Cryst. A 32 (1976) 751.
[21] F.G. Ulman, B.J. Holden, B.N. Gauguly, J.R. Hardy, Phys. Rev. B 8 (1973) 2991.
[22] S.S. Saleem, G. Aruldhas, H.D. Bist, J. Solid State Chem. 48 (1983) 77.
[23] G. Lucazeau, D. Machon, J. Raman Spectrosc. 37 (2006) 189.
[24] T. Cantunda, L.A.O. Nunes, A. Florez, Y. Messaddeq, M.A. Aegerter, Phys. Rev. B 53 (1996) 6065.
[25] M. Kusatsugu, M. Kanno, T. Honma, T. Komatsu, J. Solid State Chem. 181 (2008) 1176.
[26] M. Kanno, T. Honma, T. Komatsu, J. Am. Ceram. Soc. 92 (2009) 825.
[27] M. Kanno, T. Honma, T. Komatsu, Mater. Res. Bull. 44 (2009) 2143.
[28] Y.X. Pan, Q.Y. Zhang, Mater. Sci. Eng. B 138 (2007) 90.
[29] K. Nassau, H.J. Levinstein, G.M. Loiacono, J. Phys. Chem. Solids 26 (1965) 1805.
[30] S. Sumithra, A.M. Umarji, Solid State Sci 8 (2006) 1453.